Magnetic phase diagram of $Eu_{1-x}Ca_xCo_2P_2$ determined using muon spin rotation and relaxation

Izumi Umegaki,[1,2,3] Kodai Moriyama,[4,5] Kohei Yoshinaga,[4] Kazuki Ohishi,[6] Frank Elson,[7] Ugne Miniotaite,[7] Rasmus Palm,[7] Martin Månsson,[7] Ola Kenji Forslund,[8,9] Yasmine Sassa,[7] Soh Sugiyama,[10] Gerald D. Morris,[11] Bassam Hitti,[11] Chishiro Michioka,[4] Hiroaki Ueda,[12] Kazuyoshi Yoshimura,[4,13] and Jun Sugiyama[6,14,*]

[1]*Institute of Materials Structure Science, High Energy Accelerator Research Organization (KEK), Tokai, Ibaraki 319-1106, Japan*
[2]*Materials and Life Science Experimental Facility (MLF) Division, J-PARC Center, Tokai, Ibaraki 319-1195, Japan*
[3]*Department of Materials Structure Science, The Graduate University for Advanced Studies (SOKENDAI), Tsukuba, Ibaraki 305-0801, Japan*
[4]*Department of Chemistry, Graduate School of Science, Kyoto University, Kyoto 606-8502, Japan*
[5]*The Institute for Solid State Physics, The University of Tokyo, Kashiwa, Chiba 277-8581, Japan*
[6]*Neutron Science and Technology Center, Comprehensive Research Organization for Science and Society (CROSS), Tokai, Ibaraki 319-1106, Japan*
[7]*Department of Applied Physics, KTH Royal Institute of Technology, SE-106 91 Stockholm, Sweden*
[8]*Physik-Institut, Universität Zürich, Winterthurerstrasse 190, CH-8057 Zürich, Switzerland*
[9]*Department of Physics and Astronomy, Uppsala University, Box 516, SE-75120 Uppsala, Sweden*
[10]*Department of Physics, Nagoya University, Nagoya, Aichi 464-8602, Japan*
[11]*Centre for Molecular and Materials Science, TRIUMF, 4004 Wesbrook Mall, Vancouver, British Columbia, Canada V6T 2A3*
[12]*Institute for Advanced Materials Research and Development, Shimane University, Shimane 690-8504, Japan*
[13]*Department of Energy and Hydrocarbon Chemistry, Graduate School of Engineering, Kyoto University, Kyoto 615-8510, Japan*
[14]*Advanced Science Research Center, Japan Atomic Energy Agency, Tokai, Ibaraki 319-1195, Japan*

(Received 11 October 2023; revised 22 January 2024; accepted 18 March 2024; published 11 April 2024)

The present study investigated the magnetic nature of a solid solution system consisting of $EuCo_2P_2$ and $CaCo_2P_2$ using a muon spin rotation and relaxation (μ^+SR) technique, which is sensitive to local magnetic environments. The former compound $EuCo_2P_2$ is known to enter an incommensurate helical antiferromagnetic (AF) phase below 66 K with neutrons, which was confirmed by the present μ^+SR. The magnitude of the ordered Eu moments proposed with neutrons was found to be consistent with that estimated by μ^+SR. Furthermore, the latter lattice-collapsed tetragonal phase compound $CaCo_2P_2$ is known to enter an *A*-type AF phase below 90 K, and μ^+SR measurements on single crystals revealed the presence of a spin reorientation transition at around 40 K, below which the *A*-type AF order is likely to be completed. Although all $Eu_{1-x}Ca_xCo_2P_2$ compounds were found to enter a magnetic phase at low temperatures regardless of x, a static ordered state was formed only at the vicinity of the two end compounds, i.e., $0 \leqslant x \leqslant 0.4$ and $0.9 \leqslant x \leqslant 1$. Instead, a disordered state, i.e., a random spin-glass state, short-range ordered state, or highly fluctuating state was found in the x range between 0.4 and 0.9, even at the lowest measured temperature (2 K). Together with the magnetization data, our findings clarified the magnetic phase diagram of $Eu_{1-x}Ca_xCo_2P_2$, where a ferromagnetic exchange interaction between Co ions through the Eu^{2+} ion competes with a direct AF interaction among the Co ions, particularly in the x range between 0.57 and 0.9. This competition yielded multiple phases in $Eu_{1-x}Ca_xCo_2P_2$.

DOI: 10.1103/PhysRevB.109.144408

I. INTRODUCTION

A structural phase transition from an uncollapsed tetragonal (uc$T$) phase to a collapsed tetragonal (cT) phase in $ThCr_2Si_2$-type (see Fig. 1) compounds is known to induce a quantum-critical-point (QCP)-related unconventional phase around the phase boundary between the uc$T$ and cT phases [1–5], such as a superconducting phase in $CaFe_2As_2$ with pressure [6] and a possible QCP phase and ferromagnetic order in $SrCo_2(Ge_{1-x}P_x)_2$ with Ge doping [7]. Here, the ratio of stacking to in-plane lattice parameters (c/a) in the collapsed phase is significantly smaller than that expected from simple atomic-size considerations. Note that although both $SrCo_2P_2$ and $SrCo_2Ge_2$ are paramagnetic metals, a ferromagnetic phase appears in $SrCo_2(Ge_{1-x}P_x)_2$.

This leads to a question regarding the magnetic nature of the solid solution system between a paramagnetic uc$T$ compound, $SrCo_2P_2$, and an *A*-type antiferromagnetic (AF) cT compound, $CaCo_2P_2$, with $T_N = 90$ K [8]. Here the formal valence state of P in the uc$T$ phase is -3, while that in the cT phase is -2, i.e., $[P{-}P]^{-4}$ [9]. As a result, Co^{2+} is in a tetragonal crystal field with $S = 3/2$ ($e^4t_2^3$) in $SrCo_2P_2$, whereas Co^{1+} is with $S = 1$ ($e^4t_2^2$) in $CaCo_2P_2$ [1,9–11]. However, due to the itinerant nature of these two compounds, the effective magnetic moment (μ_{eff}) of Co in a paramagnetic state has

*juns@triumf.ca or j_sugiyama@cross.or.jp

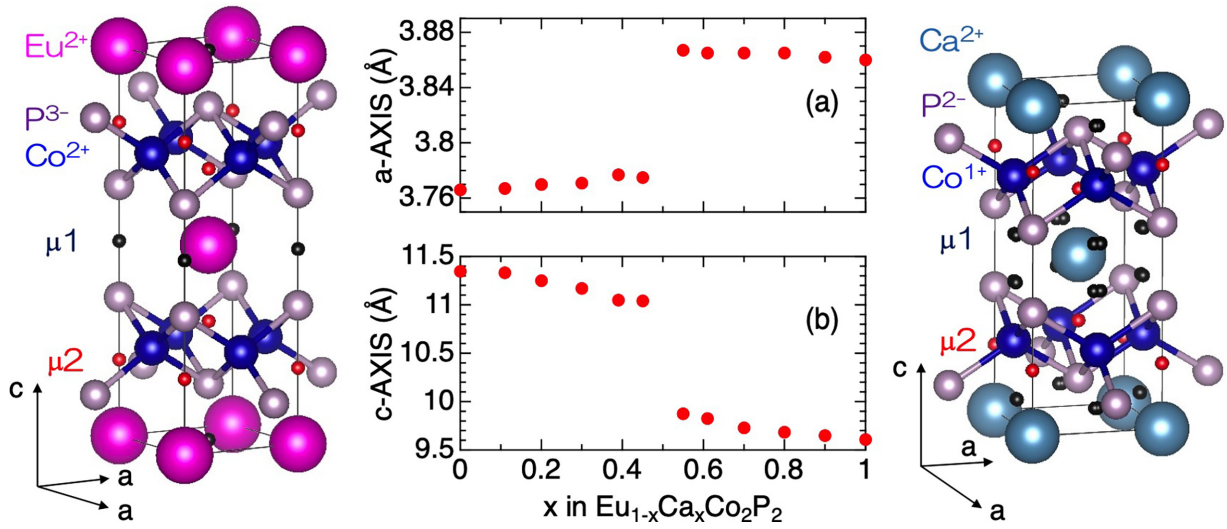

FIG. 1. Crystal structures of $EuCo_2P_2$ (left) and $CaCo_2P_2$ (right) and the lattice collapse transition in $Eu_{1-x}Ca_xCo_2P_2$, i.e., the variation of (a) the a-axis length and (b) c-axis length with the Ca content (x) [16]. In the crystal structures, two muon sites, namely, $\mu 1$ and $\mu 2$, which were predicted for $CaCo_2P_2$ and $SrCo_2P_2$ using DFT calculations [15], are also shown at (0, 0, 0.1991) and (0.5099, 0.0253, 0.0717) for $CaCo_2P_2$, and at (0, 0, 0.1954) and (0, 0, 1/2) for $EuCo_2P_2$. Note that the crystal structure and charge distribution in $EuCo_2P_2$ are the same as those in $SrCo_2P_2$.

been reported to be $1.72\,\mu_B$ for $SrCo_2P_2$ [12] and $1.1\,\mu_B$ for $CaCo_2P_2$ [13]. The previous work on $CaCo_2P_2$ [9] in the AF phase at 2 K using neutrons showed that the propagation vector $\mathbf{k} = (0, 0, 1)$, namely, the Co moments ordered ferromagnetically in the ab plane and antiferromagnetically along the c axis, i.e., A-type AF. The ordered Co moment (μ_{Co}^{ord}) was estimated to be $0.32\,\mu_B$ at 2 K. Such a small value is consistent with the metallic nature of $CaCo_2P_2$. Based on the previous nuclear magnetic resonance (NMR) [14] and muon spin rotation and relaxation (μ^+SR) [15] study, which is very sensitive to local magnetic environments, the magnetic phase diagram of $Sr_{1-x}Ca_xCo_2P_2$ exhibited the following trend: as x increases from 0, a Pauli-paramagnetic phase became stable even at 1.8 K for $0 \leqslant x \leqslant 0.45$, a short-range AF ordered phase appeared at $0.48 \leqslant x \leqslant 0.75$ with increasing T_N up to 120 K at $x = 0.75$, and, finally, a long-range AF ordered phase was formed at $x \leqslant 0.75$ with decreasing T_N down to 85 K at $x = 1$. Thus, the highest T_N was not observed for the pure compound with $x = 1$, i.e., $CaCo_2P_2$, but was instead observed for the $x = 0.75$ compound, around which the lattice collapse transition occurred. This clearly suggests the interrelationship among the Co-Co distance along the c axis, the AF interaction, and the increase in the magnetic Co^{1+} caused by the substitution of Sr by Ca. In order to further understand this interrelationship, we attempted to expand the μ^+SR study to a solid solution system between two AF materials, namely, an AF-uc$T$ compound, $EuCo_2P_2$ [17–21], and an AF-cT compound, $CaCo_2P_2$ (see Fig. 1) [16]. The previous neutron work revealed that $EuCo_2P_2$ enters an incommensurate helical AF phase below $T_N = 66.5(2)$ K [17]. Only the Eu^{2+} moments order with the propagation vector $\mathbf{k} = (0, 0, 0.85)$ and the ordered magnetic moment (μ_{Eu}^{ord}) of $6.9(1)\,\mu_B$ at 15 K. Consequently, each Eu moment aligns in the ab plane ferromagnetically, while the Eu moments order along the c axis to form an incommensurate AF spiral structure with a modulation period of $\sim c/0.85 = \sim 1.18c$.

Hence, besides the transition from a uc$T$ phase to a cT phase, the magnetic nature in $Eu_{1-x}Ca_xCo_2P_2$ is strongly affected by the interactions among the Eu moments in the low-x region, which is in turn governed by the interactions among the Co moments in the high-x region. In addition, the interaction between Eu moments and Co moments plays a significant role in the total magnetic nature. In fact, magnetization measurements showed a complex magnetic phase diagram for $Eu_{1-x}Ca_xCo_2P_2$ [16]. More specifically, as x increased from 0, T_N decreased with x from 66.5 K at $x = 0$ to 44 K at $x = 0.45$, and a ferromagnetic phase appeared below 212 K ($= T_C$) at $x = 0.52$, T_C decreased with x down to 126 K at $x = 0.85$, and then another AF phase appeared below $T_N = 108$ K at $x = 1$. In the region with $x > 0.5$, a second magnetic transition was detected at 71 K for the $x = 0.52$ sample, and the transition temperature decreased with x, reaching a minimum value of around 17 K for the $x = 0.85$ sample. However, the detailed nature of the second transition and the phases appearing in the phase diagram are still not clearly understood. Therefore, we have used μ^+SR to further understand the magnetic phases in $Eu_{1-x}Ca_xCo_2P_2$.

II. EXPERIMENTAL SETUP

Polycrystalline samples of $Eu_{1-x}Ca_xCo_2P_2$ with $x = 0-1$ were prepared from P, Eu, Ca, and Co using a two-step reaction. For the first step, EuP, CaP, and Co_2P were synthesized through a solid-state reaction between Eu (Ca, Co) and P in an evacuated quartz tube at 800 °C (700 °C for Co_2P). In the second step, $Eu_{1-x}Ca_xCo_2P_2$ were synthesized through a solid-state reaction among EuP, CaP and Co_2P at 1000 °C for 20 h in an Ar atmosphere. After grinding, the obtained powder was annealed two times at 1000 °C for 40 hours in an Ar atmosphere [16].

Single-crystal platelet samples were prepared by a Sn-flux method [21,22]. A mixture of Eu, Ca, Co, P, and Sn with a

molar ratio of $1.5(1-x) : 1.5x : 2 : 2 : 40$ was sealed into a quartz tube in an Ar atmosphere at 0.33 atm. The quartz tube was heated to 1150 °C, kept for 40 h, and cooled down to 600 °C with a cooling rate of 3°/h, and then further cooled down to room temperature within 6 h. The Sn flux was removed by rinsing with acid after a centrifuge. The typical dimension of a single-crystal platelet was approximately $0.5 \times 0.5 \times 0.1$ mm^3. The basal plane was assigned as a c plane.

According to powder x-ray diffraction (XRD) analyses, all samples were almost a single phase of tetragonal symmetry with a space group of $I4/mmm$, as explained in Sec. III. Also, as x increased from 0, the c-axis length monotonically decreased with x until ∼0.5. Consequently, it rapidly decreased down to 0.9 and, finally, reached a constant value above $x = 0.9$. It should be mentioned that this behavior is consistent with the one described in the literature. Magnetization measurements suggested the presence of a magnetic transition above $T \sim 60$ K for samples with $x \geqslant 0.5$.

The μ^+SR spectra were measured at surface muon beam lines using the LAMPF spectrometer on the M20 beam line of TRIUMF in Canada. Approximately 200 mg of powder sample was placed in an envelope with an area of 1×1 cm^2, made of 0.05-mm-thick Al-coated Mylar tape to minimize the background signal from the envelope. Pertaining to the single-crystal platelets, about 50 platelets were aligned on a Ag plate with an area of 1×1 cm^2 by an Apiezon wax so as to form a mosaic c plane. Then, the envelope or the Ag plate was attached to a low-background sample holder in a liquid-He flow-type cryostat for measurements in the T range between 1.8 and 150 K. The experimental techniques are described in more detail elsewhere [23–25]. The recorded μ^+SR spectrum was analyzed with MUSRFIT [26].

III. RESULTS

Initially, the μ^+SR measurement in a weak transverse field (wTF) determined the presence of a magnetic transition temperature of each compound with $x = 0-1$. Here, "weak" indicates that the applied magnetic field is very small compared with the internal magnetic field, and "transverse" refers to a field that is perpendicular to the initial muon spin polarization. The muon spin precesses with wTF in a paramagnetic state, while such a wTF precession signal is suppressed in a magnetic state due to a large internal magnetic field, as shown in Fig. 2. The wTF-μ^+SR spectrum was fitted using a combination of an exponentially relaxing cosine oscillation and an exponentially relaxing nonoscillatory signal caused by the formation of a magnetic ordered phase, as follows:

$$A_0 P_{\rm TF}(t) = A_{\rm TF} \cos(2\pi f_{\rm TF} t + \phi_{\rm TF}) \exp(-\lambda_{\rm TF} t) + A_{\rm M} \exp(-\lambda_{\rm M} t), \quad (1)$$

where A_0 denotes the initial asymmetry at $t = 0$, $P_{\rm TF}(t)$ denotes the muon spin depolarization function in the TF, $A_{\rm TF}$ and $A_{\rm M}$ denote the asymmetries of the two signals, $f_{\rm TF}$ and $\phi_{\rm TF}$ denote the muon spin precession frequency and the initial phase of the precession due to TF, respectively, and $\lambda_{\rm TF}$ and $\lambda_{\rm M}$ denote the exponential relaxation rates for the two signals. Figure 3 demonstrates the temperature dependence of $A_{\rm TF}$ for each sample. Since $A_{\rm TF}$ is roughly proportional to the volume fraction of paramagnetic phases in a sample, a steplike change in each $A_{\rm TF}(T)$ curve indicates that each sample enters a magnetic phase at low temperatures. The transition temperature was estimated by fitting the $A_{\rm TF}(T)$ curve with a Sigmoid function. As x increases, the transition temperature decreases from 67.9 to 48.9 K, then leaps up to 214 K at $x = 0.6$, and

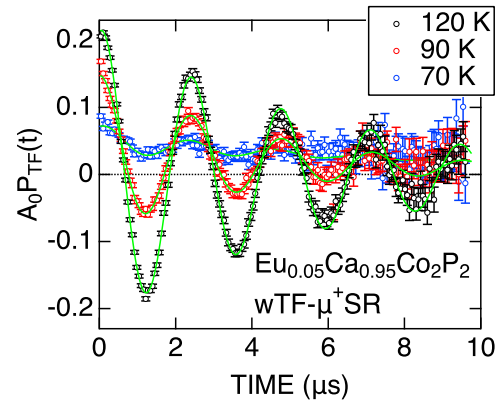

FIG. 2. The temperature variation of the wTF-μ^+SR spectrum for $Eu_{0.05}Ca_{0.95}Co_2P_2$. The magnitude of the TF was 30 Oe.

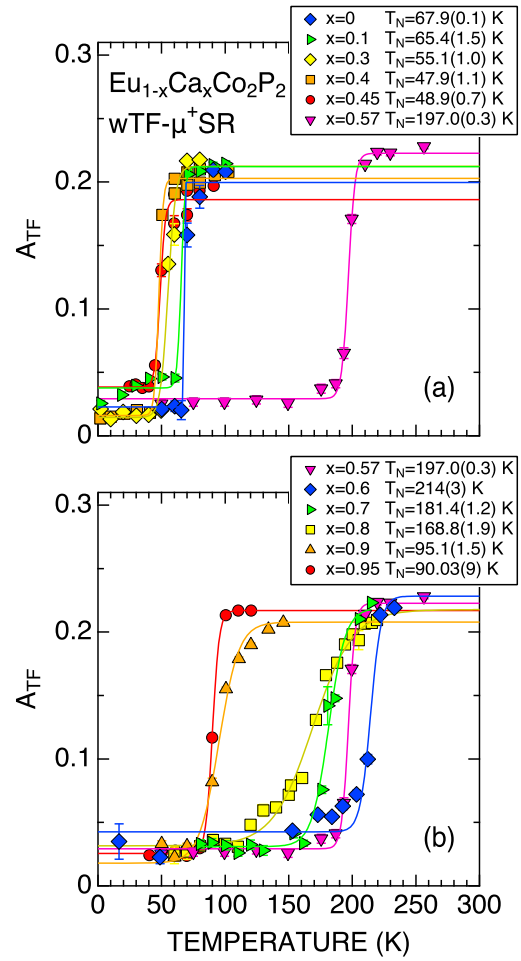

FIG. 3. The temperature dependence of the wTF asymmetry ($A_{\rm TF}$) for the 11 $Eu_{1-x}Ca_xCo_2P_2$ samples. The data were obtained by fitting the wTF-μ^+SR spectrum with Eq. (1).

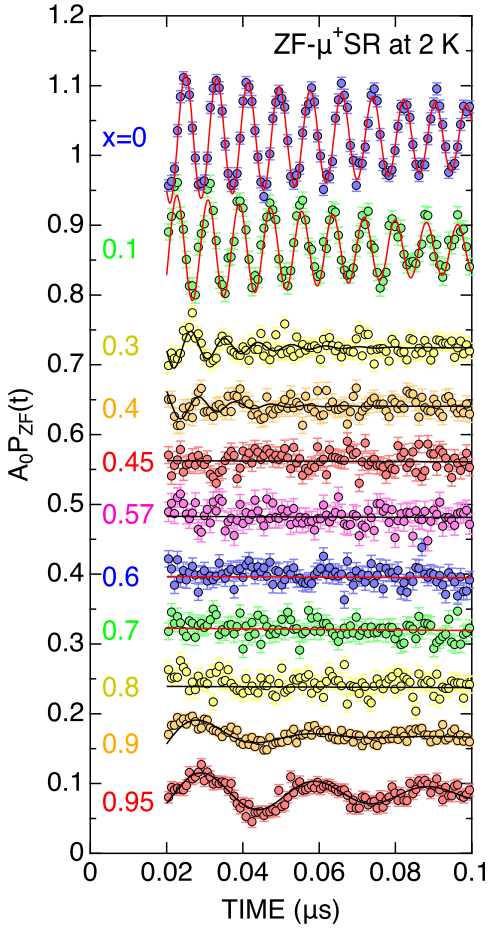

FIG. 4. The variation of the ZF-μ^+SR spectrum for $Eu_{1-x}Ca_xCo_2P_2$ with the Ca content (x) recorded at 2 K using a powder sample. For clarity of display, each spectrum is shifted upward by 0.08. Only the spectra for the $x = 0.1$ and 0 compounds are shifted upward by 0.16.

then rapidly decreases with further increasing x (see, also Fig. 14).

It should be noted that A_{TF} of each sample is nonzero, even below T_N. More correctly, A_{TF} well below T_N ranges between around 0.02 to 0.03, indicating the presence of nonmagnetic impurity phases in the sample. Since the maximum A_{TF} is about 0.24, the volume fraction of such nonmagnetic impurity phases is estimated as 8–13%. In other words, about 90% of each sample is found to be a single phase of $Eu_{1-x}Ca_xCo_2P_2$. Next, to understand the nature of the low-temperature magnetic phase of each $Eu_{1-x}Ca_xCo_2P_2$ sample, Fig. 4 shows the zero-field (ZF) μ^+SR spectra for each sample recorded at the lowest temperature reached with the present setup, i.e., 2 K, which is well below the magnetic transition temperature detected by wTF-μ^+SR (see Fig. 3). Although the ZF spectrum for the $x = 0$ sample, i.e., $EuCo_2P_2$, exhibited a clear oscillatory signal at 2 K, such signal is suppressed with x and disappears at $x > 0.4$. For the sample with $x = 0.45$–0.8, the ZF spectrum lacks an oscillatory signal but exhibits a fast relaxing behavior, indicating the presence of a large fluctuating internal magnetic field or a large random internal magnetic field. At present, since it is difficult to distinguish the former from the latter, we will call such phase a *disordered (DO) phase*, which includes a random spin-glass phase, short-range ordered phase, and highly fluctuating phase, with respect to the μ^+SR time window and spatial resolution.

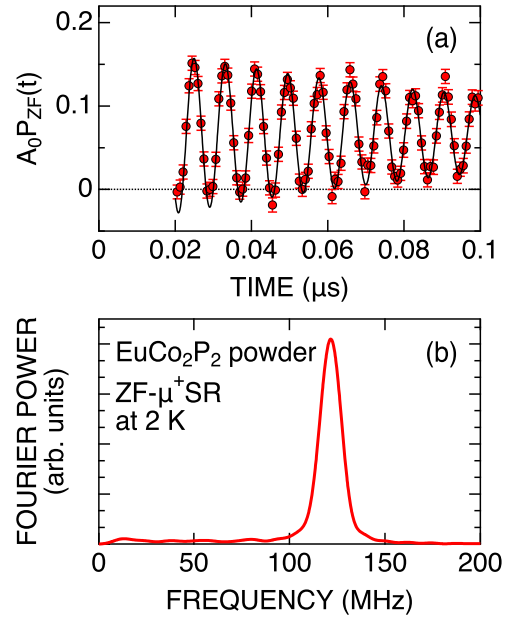

FIG. 5. (a) The ZF-μ^+SR time spectrum for $EuCo_2P_2$ recorded at 2 K and (b) the Fourier transform frequency spectrum of (a). The spectrum in (a) is the same as the top spectrum shown in Fig. 4.

As x increases further than $x = 0.8$, a damped oscillation is observed in the ZF spectrum for the $x = 0.9$ sample, which is enhanced with x, while a clear oscillation is observed in the ZF spectrum for the sample with $x \geqslant 0.9$.

These features clearly suggest that a static magnetic order is formed only at the x region close to $x = 0$ and $x = 1$, i.e., $0 \leqslant x < 0.45$ and $0.8 < x \leqslant 1$, even at 2 K. In the intermediate-x region with $0.45 \leqslant x \leqslant 0.8$, the ground state is magnetic but not static ordered, i.e., DO. The next section presents the results from each examined sample.

A. $EuCo_2P_2$

The previous powder neutron diffraction experiments have described the magnetic ground state of one of the two end members, $EuCo_2P_2$, as an incommensurate helical AF ordered state [17]. Thus, the ZF-μ^+SR spectrum is naively expected to exhibit a damped oscillation with a wide field distribution and large initial phase delay, represented by the zeroth-order Bessel function of the first kind [23,27,28]. Nevertheless, the ZF-μ^+SR spectrum exhibited a clear oscillation with a sharp distribution (see Fig. 5) and it can thus be well fitted with a combination of an exponentially relaxing cosine oscillation without a large phase delay and an exponentially relaxing nonoscillatory signal, as follows:

$$A_0 P_{ZF}(t) = A_{AF}\cos(2\pi f_{AF} t + \phi_{AF})\exp(-\lambda_{AF} t) + A_{tail}\exp(-\lambda_{tail} t), \quad (2)$$

where $P_{ZF}(t)$ denotes the muon spin depolarization function in ZF, A_{AF} and A_{tail} denote the asymmetries of the two signals, f_{AF} and ϕ_{AF} denote the muon spin precession frequency and

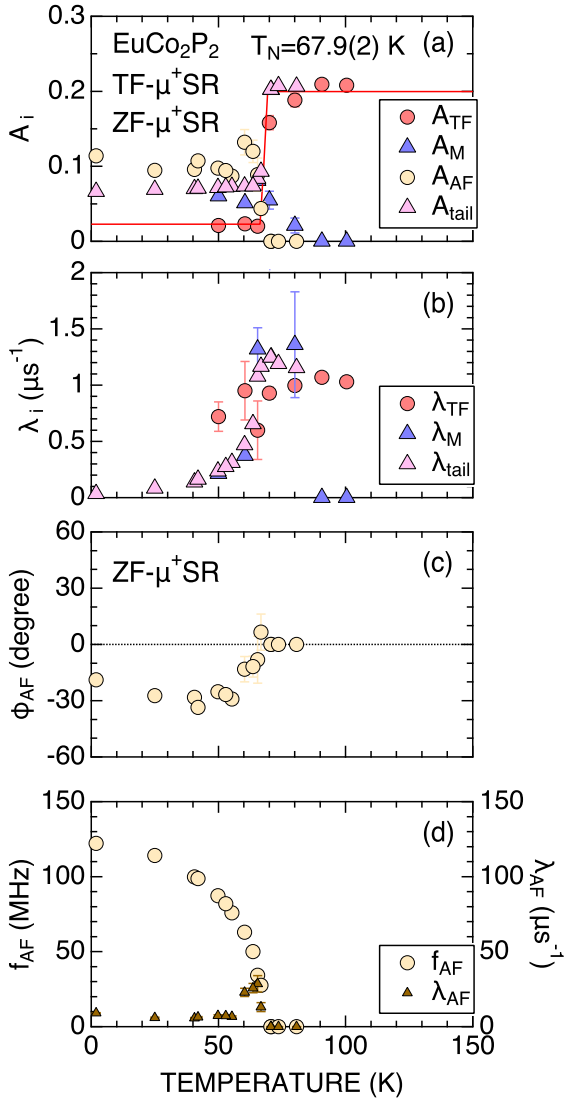

FIG. 6. (a) The temperature dependencies of the TF- and ZF-μ^+SR parameters for $EuCo_2P_2$: (a) asymmetries (A_i), (b) relaxation rates (λ_i), (c) initial phase of the precession signal (ϕ_{AF}), and (d) muon spin precession frequency and its relaxation rate (f_{AF} and λ_{AF}). The data were obtained by fitting the TF-μ^+SR spectrum with Eq. (1) and the ZF-μ^+SR spectrum with Eq. (2).

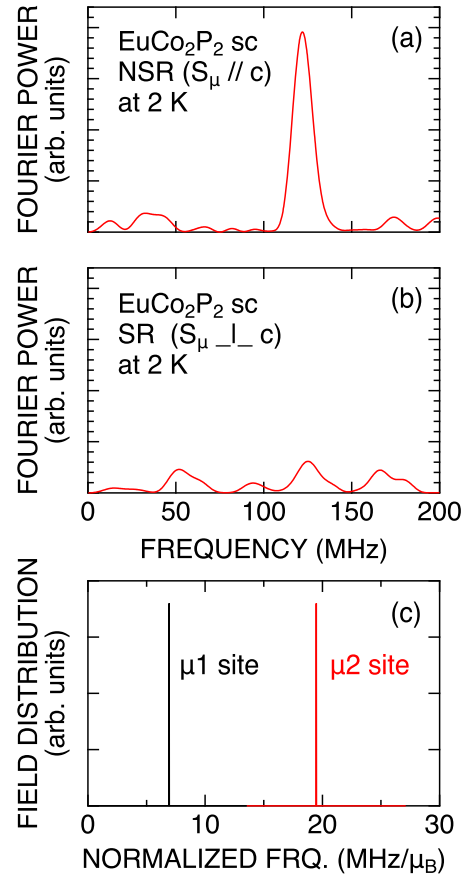

FIG. 7. The Fourier transform frequency spectrum of the ZF-μ^+SR time spectrum recorded at 2 K using (a) backward and forward counters with a non-spin-rotating (NSR) mode where $\boldsymbol{S_\mu} \parallel \boldsymbol{c}$ and (b) up and down counters with a spin-rotating (SR) mode where $\boldsymbol{S_\mu} \perp \boldsymbol{c}$ for $EuCo_2P_2$ single-crystal platelets aligned on an Ag plate. That is, the crystals were aligned so that the c axis is perpendicular to the Ag plate, i.e., a mosaic c plane was formed. (c) The field distribution at the two muon sites, namely, $\mu 1$ (0,0,0.1954) and $\mu 2$ (0,0,1/2), that were predicted with dipole field calculations using MUESR [29].

the initial phase of the precession due to the internal magnetic field, respectively, and λ_{AF} and λ_{tail} denote the exponential relaxation rates for the two signals. Since $A_{tail} \sim \frac{1}{2}A_{AF}$ at 2 K, the A_{tail} signal is assigned as a powder "1/3 tail" signal caused by μ^+, for which the initial muon spin ($\boldsymbol{S_\mu}$) is parallel to the internal magnetic field. Figure 6 shows the temperature dependencies of the wTF and ZF-μ^+SR parameters for $EuCo_2P_2$. The relaxation rate of the A_{tail} signal (λ_{tail}) decreases with decreasing temperature, approaching a zero value at 0 K, as expected for the tail signal [Fig. 6(b)]. The initial phase of the oscillatory signal (ϕ_{AF}) ranges between 0 and -30° below T_N and $\phi_{AF} = -18.9(1.6)$ deg at 2 K [Fig. 6(c)]. Considering that $f_{AF} \sim 120$ MHz at 2 K [see Fig. 5(b)], the phase delay of 18.9 deg corresponds to 0.438 ns $= 1/(120 \times 10^6) \times 18.9/360$ sec, which is comparable to the bin size of the time digital converter (TDC), i.e., 0.390 ns in the present setup. This in turn means that it is difficult to determine the phase delay correctly. The $f_{AF}(T)$ curve exhibits an order parameterlike temperature dependence. λ_{AF} shows a critical behavior below the vicinity of T_N, while λ_{AF} becomes very small and almost temperature independent below 60 K. Overall, the internal magnetic field ($\boldsymbol{H}_{\mathbf{int}}$) detected with μ^+SR is unlikely to confirm the formation of an incommensurate magnetic order. To further understand $\boldsymbol{H}_{\mathbf{int}}$, Fig. 7 demonstrates the Fourier transform frequency spectrum of the ZF-μ^+SR time spectrum for the $EuCo_2P_2$ single crystals, which were aligned on an Ag plate so that the c axis is perpendicular to the Ag plate. Using a non-spin-rotating (NSR) mode with $\boldsymbol{S_\mu} \parallel \boldsymbol{c}$, a clear oscillation was observed at approximately 120 MHz. In contrast, such an oscillation was not observed using a spin-rotating (SR) mode with $\boldsymbol{S_\mu} \perp \boldsymbol{c}$. The muon spin naturally starts to precess when the internal magnetic field ($\boldsymbol{H}_{\mathbf{int}}$) is perpendicular to $\boldsymbol{S_\mu}$ ($\boldsymbol{H}_{\mathbf{int}} \perp \boldsymbol{c}$), leading to $\boldsymbol{H}_{\mathbf{int}} \perp \boldsymbol{S_\mu}$. In such case, the distribution at the muon site cannot be explained by a Bessel function, but instead by a cosine function, depending on the muon site [24].

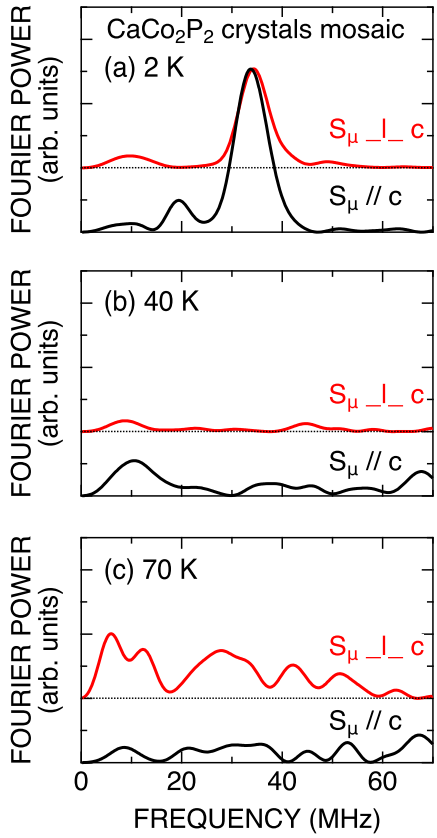

FIG. 8. The Fourier transform frequency spectrum of the ZF-μ^+SR time spectrum for $CaCo_2P_2$ single-crystal platelets aligned on an Ag plate to form a mosaic c plane. The ZF-μ^+SR spectrum was recorded at (a) 2 K, (b) 40 K, and (c) 70 K.

In fact, Fig. 7(c) shows the field distributions at the two predicted muon sites in the incommensurate helical AF ordered state with $\mathbf{k} = (0, 0, 0.85)$ obtained by dipole field calculations using MUESR [29]. A comparison between Fig. 7(c) and Figs. 5(b) and 7(a) enables the estimation of the ordered Eu moment ($\mu_{\rm Eu}^{\rm ord}$) at 2 K as 17.53 $\mu_{\rm B}$, when the implanted muons sit at the $\mu1$ site. On the contrary, $\mu_{\rm Eu}^{\rm ord} = 6.24\,\mu_{\rm B}$, when the implanted muons sit at the $\mu2$ site. Since the former value is too large for Eu, the implanted muons are found to sit at the $\mu2$ site. In fact, the density functional theory (DFT) calculations predicted that the $\mu2$ site is slightly more stable than the $\mu1$ site. The μ^+SR-estimated $\mu_{\rm Eu}^{\rm ord}$ is consistent with the previously reported value by neutron ($\mu_{\rm Eu}^{\rm ord} = 6.9(1)\,\mu_{\rm B}$ at 15 K [17]).

B. $CaCo_2P_2$

The magnetic anisotropy in the ordered state of the other end member compound $CaCo_2P_2$ was also studied with ZF-μ^+SR using single-crystal platelets, while the detailed μ^+SR result on a powder sample has already been reported in our previous work [15,30]. Figure 8 shows the Fourier transform frequency spectrum of the ZF-μ^+SR time spectrum for aligned $CaCo_2P_2$ single-crystal platelets recorded at 2, 40, and 70 K. At 2 K, $\boldsymbol{H}_{\rm int}$ is found to have both components in the ab plane and along the c axis. In fact, fitting of the two ZF-μ^+SR time spectra, i.e., the spectra recorded at 2 K with NSR and SR modes, with Eq. (2) revealed that the angle of $\boldsymbol{H}_{\rm int}$ from the ab plane is approximately 45 deg. On the contrary, there is mainly one component in the ab plane at 40 K and along the c axis at 70 K, indicating that the direction of $\boldsymbol{H}_{\rm int}$ changes with temperature below $T_{\rm N}$. Such change was also observed at approximately 40 K by NMR [31].

Furthermore, dipole field calculations on $CaCo_2P_2$ revealed that $\boldsymbol{H}_{\rm int}$ at the $\mu2$ site (0,0,0.1991) lies in the ab plane for the proposed A-type AF structure, while $\boldsymbol{H}_{\rm int}$ at the $\mu1$ site (0.5099,0.0253,0.0717) is canted along the c axis by about 10 deg. It is difficult to explain the magnitude of $\boldsymbol{H}_{\rm int}$ using the ordered Co moment determined by neutron (0.32 $\mu_{\rm B}$). More specifically, the simple dipole field calculations for the A-type AF ordered state provided that $f_{\rm AF} = 13$ MHz for the $\mu1$ site and 4 MHz for the $\mu2$ site [15], suggesting that it is necessary to consider a hyperfine coupling field caused by the local spin density at the muon site [24,32,33], even for the A-type AF case [34], because Co^{1+} ions in each layer align ferromagnetically. In the previous neutron work [9], the neutron diffraction pattern was measured only at three distinct temperatures, i.e., 420, 270, and 2 K, and only one magnetic diffraction peak, assigned as (001), was observed at 2 K. Considering the change in the direction of $\boldsymbol{H}_{\rm int}$ with temperature below $T_{\rm N}$, it is highly preferable to measure the temperature dependence of the neutron diffraction pattern for $CaCo_2P_2$ below $T_{\rm N}$.

C. $Eu_{1-x}Ca_xCo_2P_2$ with $0 < x \leqslant 0.45$

In this x range, a clear oscillation can be observed for the compounds with $x \leqslant 0.4$. This is an oscillation which, however, disappears, giving rise to a relaxation signal instead for the compound with $0.4 < x = 0.45$ (Fig. 4). The ZF spectrum was thus fitted by Eq. (2) together with an exponentially relaxation signal,

$$A_0 P_{\rm ZF}(t) = A_{\rm AF}\cos(2\pi f_{\rm AF} t + \phi_{\rm AF})\exp(-\lambda_{\rm AF} t) + A_{\rm tail}\exp(-\lambda_{\rm tail} t) + A_{\rm F}\exp(-\lambda_{\rm F} t), \quad (3)$$

where $A_{\rm F}$ and $\lambda_{\rm F}$ denote the asymmetry and relaxation rate, respectively, of the additional exponential relaxation signal. Note that $A_{\rm F} = 0$ for the $x = 0.1$ compound.

Figure 9 shows the temperature dependencies of the oscillation frequency ($f_{\rm AF}$) and its relaxation rate ($\lambda_{\rm AF}$) for the $x = 0-0.4$ compounds. Both $f_{\rm AF}(T)$ and $\lambda_{\rm AF}(T)$ curves for the $x = 0.1$ compound are almost identical to those for the $x = 0$ compound, i.e., $EuCo_2P_2$. However, as x increases further than 0.1, the magnitude of $f_{\rm AF}$ at 2 K begins to decrease slightly, while $\lambda_{\rm AF}$ increases drastically. As a result, the oscillatory signal disappears for the $x = 0.3$ (0.4) compound at around 60 K (30 K), where $\lambda_{\rm AF} > f_{\rm AF}$. Note that the wTF-$\mu^+$SR measurements revealed that $T_{\rm N} = 47.9(1.1)$ K for the $x = 0.4$ compound, indicating the presence of a disordered phase at temperatures between $T_{\rm N}$ and 30 K. In contrast, the ZF spectrum for the $0.4 < x$ compounds lacks a clear oscillation, indicating the absence of a static magnetic order. The ZF spectrum was fitted with a combination of two exponentially relaxation functions, i.e., fast and slowly relaxing signals, as follows:

$$A_0 P_{\rm ZF}(t) = A_{\rm F}\exp(-\lambda_{\rm F} t) + A_{\rm S}\exp(-\lambda_{\rm S} t), \quad (4)$$

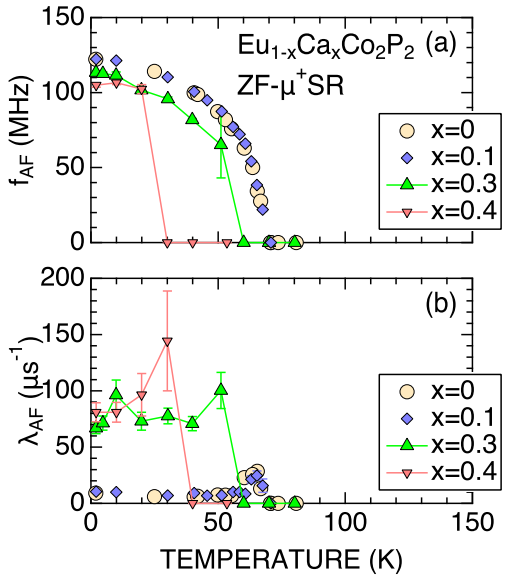

FIG. 9. The temperature dependencies of (a) the muon spin precession frequency (f_{AF}) and (b) the relaxation rate (λ_{AF}) for $Eu_{1-x}Ca_xCo_2P_2$ with $x = 0-0.4$. The data were obtained by fitting the ZF-μ^+SR spectra with Eq. (3).

where A_F and A_S denote the asymmetries of the two signals, and λ_F and λ_S denote their exponential relaxation rates.

Figure 10 shows the temperature dependencies of the wTF- and ZF-μ^+SR parameters for the $x = 0.45$ compound. The A_M signal in the TF spectrum is found to correspond to the A_S signal, which is also assumed to be the longitudinal component of the fluctuating $\boldsymbol{H}_{\mathbf{int}}$ due to the fact that $\lambda_S < \lambda_F$ and λ_S approaches zero with $T \to 0$, i.e., the 1/3 tail signal shown in Fig. 6. On the contrary, the A_F signal should correspond to the transverse component of the fluctuating $\boldsymbol{H}_{\mathbf{int}}$, while A_F is smaller than the expected value ($2A_S$), as seen in Fig. 10(a).

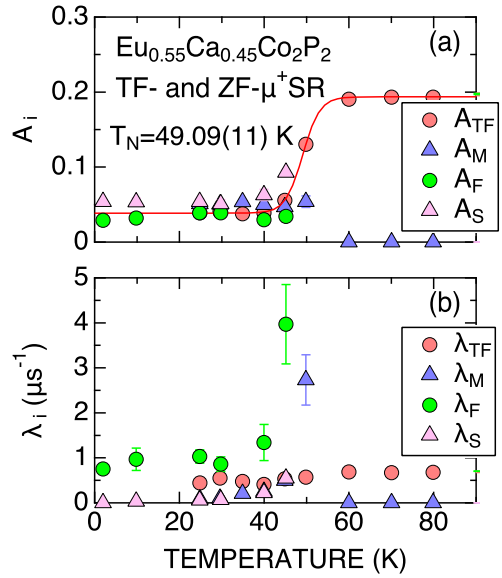

FIG. 10. The temperature dependencies of the TF- and ZF-μ^+SR parameters for $Eu_{0.55}Ca_{0.45}Co_2P_2$. The data were obtained by fitting the TF- and ZF-μ^+SR spectra with Eqs. (1) and (4).

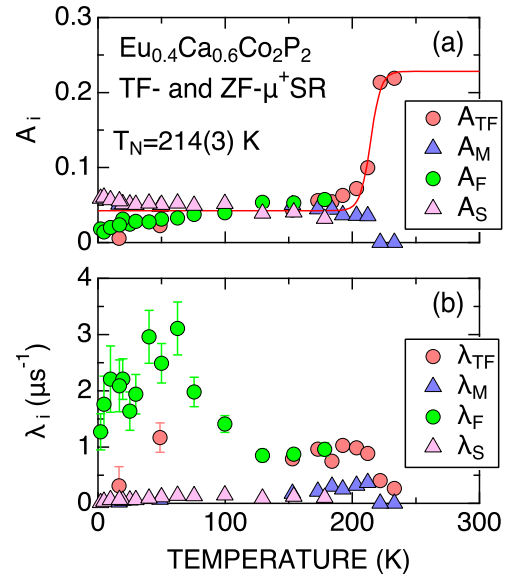

FIG. 11. The temperature dependencies of the TF- and ZF-μ^+SR parameters for $Eu_{0.4}Ca_{0.6}Co_2P_2$. The data were obtained by fitting the TF- and ZF-μ^+SR spectra with Eqs. (1) and (4).

This would suggest the presence of a very rapidly relaxing signal in an early time domain below 0.02 μs (see Fig. 4), which is not visible in the present μ^+SR setup. Note that a muonium (μ^+e^-) state, for which the gyromagnetic ratio is 100 times larger than that of μ^+, is highly unlikely to be present in the compound due to the metallic nature of this system. To further investigate the magnetic ground state of this compound, neutron scattering experiments are highly preferable due to the faster time window of neutrons than muons. Besides that, both $\lambda_F(T)$ and $\lambda_S(T)$ curves exhibit a monotonic change with temperature, indicating the absence of a second magnetic transition below T_N.

Overall, the compounds with $0.4 < x$ were found to enter a magnetic phase without a static magnetic order; however, the nature of this phase is still not clearly understood owing to the limited time window of μ^+SR, i.e., lack of information in the time domain $t < 0.02$ μs.

D. $Eu_{1-x}Ca_xCo_2P_2$ with $0.57 \leqslant x \leqslant 0.8$

Although the ZF-μ^+SR spectrum for the compounds in this x range lacks an oscillation, it exhibits a distinct relaxation behavior even at 2 K, similar to the $x = 0.45$ compound. This spectrum was also fitted with Eq. (4). Figure 11 shows the temperature dependencies of the TF- and ZF-μ^+SR parameters for $Eu_{0.4}Ca_{0.6}Co_2P_2$. Despite the fact that the overall behavior of each parameter is similar to that for the $0.4 < x \leqslant 0.45$ compounds, the $\lambda_F(T)$ curve exhibits a broad maximum at around 50 K [Fig. 11(b)]. Generally, λ_i's in a magnetic phase are expected to decrease with decreasing temperature (see Fig. 6) due to the suppression of thermal magnetic fluctuations, except below the vicinity of the magnetic transition temperature. Therefore, the increase in λ_F with decreasing temperature noted between 120 and 50 K most likely indicates a critical behavior of the fluctuation that is associated with a second magnetic transition below $T_N = 214(3)$ K. Moreover,

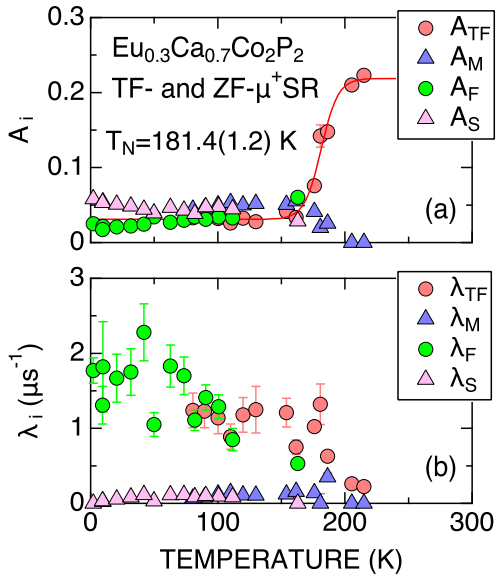

FIG. 12. The temperature dependencies of the TF- and ZF-μ^+SR parameters for $Eu_{0.3}Ca_{0.7}Co_2P_2$. The data were obtained by fitting the TF- and ZF-μ^+SR spectra with Eqs. (1) and (4).

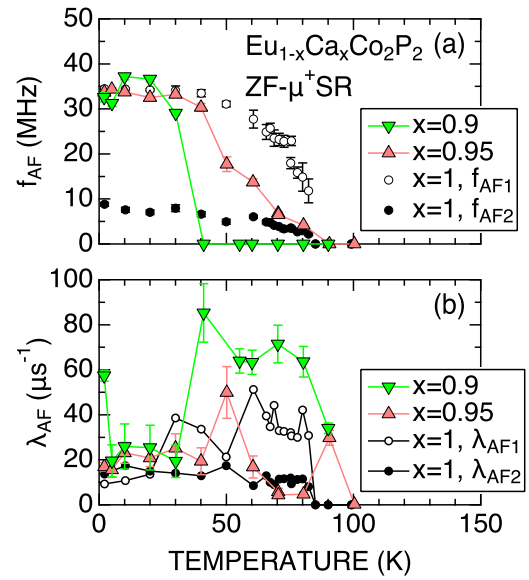

FIG. 13. The temperature dependencies of (a) the muon spin precession frequency (f_{AF}) and (b) the relaxation rate (λ_{AF}) for $Eu_{1-x}Ca_xCo_2P_2$ with $x = 0.9$, 0.95, and 1. The data were obtained by fitting the ZF-μ^+SR spectra with Eq. (2), while the data for the $x = 1$ sample, $CaCo_2P_2$, were obtained by fitting the ZF-μ^+SR spectra with Eq. (2) and one more oscillatory signal [15]. The data for the $x = 1$ sample are the same as in Ref. [15].

since no anomaly is observed in the $\lambda_S(T)$ curve at around 50 K, the second magnetic transition is unlikely to drastically alter the local magnetic environments. A similar behavior was also observed in the $\lambda_F(T)$ curve for $Eu_{0.3}Ca_{0.7}Co_2P_2$ at around 50 K [Fig. 12(b)]. Consequently, even for compounds without a clear precession signal in the ZF-μ^+SR spectrum, a second magnetic transition temperature could be determined from the temperature dependence of the relaxation rate together with the magnetization measurements. However, the absence of a precession signal indicates the presence of a DO phase even at 2 K for compounds in this x range as well.

E. $Eu_{1-x}Ca_xCo_2P_2$ with $0.8 < x < 1$

Although the end compound, $CaCo_2P_2$, exhibits a clear oscillation consisting of two different frequency components [15], only one oscillatory component was observed in the $x \geqslant 0.95$ compound due to the inhomogeneous local magnetic environments caused by the Ca substitution for Eu. Figure 13 shows the temperature dependencies of the oscillatory frequency (f_{AF}) and its relaxation rate (λ_{AF}) for the $x = 0.95$ and 0.9 compounds together with the results obtained for the $x = 1$ compound [15]. Since the direction of $\boldsymbol{H}_{\mathbf{int}}$ in $CaCo_2P_2$ changes at approximately 40 K (Fig. 8), the predominant signal will also change accordingly from a low-temperature 35 MHz component (f_{AF1}) to a high-temperature 10 MHz component (f_{AF2}). This also results in the increase in λ_{AF1} above 50 K.

Such behavior is also observed in the $f_{AF}(T)$ and $\lambda_{AF}(T)$ curves for the $x = 0.95$ compound, while there is only one oscillatory component. For the $x = 0.9$ compound, the oscillatory signal disappears over 40 K because λ_{AF} is larger than f_{AF}, particularly above that temperature. Overall, the direction of $\boldsymbol{H}_{\mathbf{int}}$ is found to change at approximately 40 K in the compound with $0.8 \leqslant x \leqslant 1$, and based on the local maximum shown in the $\lambda_{AF}(T)$ curve [$\lambda_{AF1}(T)$ curve for the $x = 1$ compound] below 50 K, such direction change occurs at $T_{DC} = 30$ K for $CaCo_2P_2$, 20 K for the $x = 0.95$ compound, and perhaps 15 K for the $x = 0.9$ compound.

IV. DISCUSSION

A. Magnetic phase diagram

Although μ^+SR can detect a magnetic transition temperature and distribution of internal magnetic field in a sample, it is difficult to determine whether the magnetic order is ferromagnetic or antiferromagnetic. Therefore, the magnetic phase diagram of $Eu_{1-x}Ca_xCo_2P_2$ is drawn using the present μ^+SR result, but also the previous magnetization measurements [16] (Fig. 14). It should be emphasized again that the "DO phase" refers to the phase in which a clear muon spin precession signal could not be observed down to 2 K, while a large internal magnetic field exists. The DO phase thus includes a static spin-glass phase, a dynamic spin-glass phase, a static short-range ordered phase, or a dynamic short-range ordered phase. As x increases from 0, an incommensurate AF (IC-AF) phase exists until $x = 0.4$, then an DO-AF phase appears up to $x = 0.9$, and then an A-type AF phase is formed at $x > 0.9$. The transition temperature for these three AF phases (T_N) decreases gradually down to 15 K with increasing x until $x = 0.9$, and then increases up to approximately 40 K at $x = 1$. In addition, as x increases from 0, a DO-ferromagnetic (FM) phase suddenly appears at approximately $x = 0.57$ ($T_C \sim 200$ K), around which the lattice collapse transition occurs, T_C reaches a maximum [214(3) K] at $x = 0.6$, and T_C decreases with further increasing x. Finally, this DO-FM phase disappears at $x = 0.9$, giving its place to an AF phase. Therefore, for compounds with $0.9 \leqslant x$, when the temperature decreases

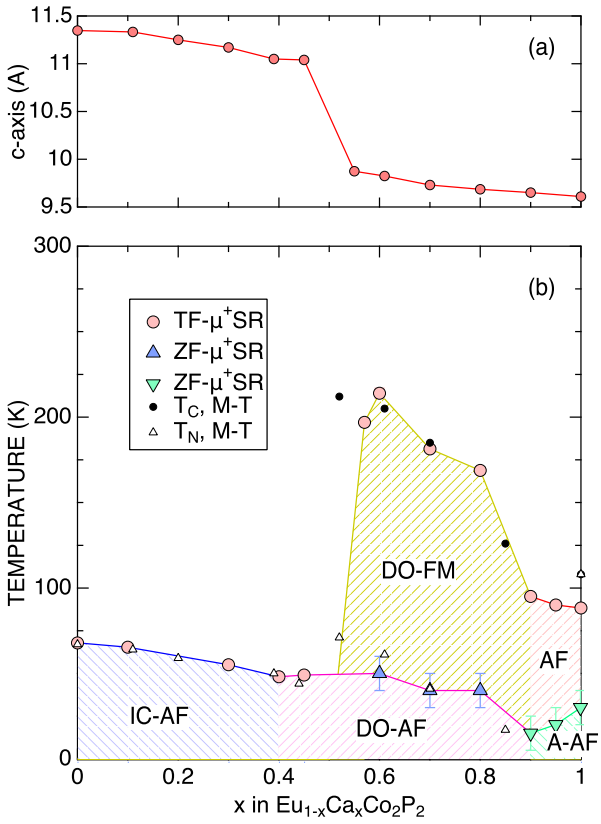

FIG. 14. (a) The change in the c-axis length with x and (b) magnetic phase diagram of $Eu_{1-x}Ca_xCo_2P_2$ determined by μ^+SR and magnetization measurements. In (b), AF, A-AF, DO-FM, DO-AF, and IC-AF denote an AF ordered phase, A-type AF ordered phase, disordered ferromagnetic phase, disordered AF phase, and incommensurate AF ordered phase, respectively. (a) is the same as Fig. 1(b) to emphasize the interrelationship between the structural phase transition and magnetic phase diagram.

below 300 K, the compound enters the AF phase at approximately 90 K, which is in turn completed below 15–40 K. This indicates the presence of a spin reorientation transition in this x range below 15–40 K that is dependent on x. Consequently, we definitely need a neutron diffraction experiment on $Eu_{1-x}Ca_xCo_2P_2$ with $0.9 \leqslant x$ to further understand a spin reorientation behavior.

The discrepancy of T_N in $CaCo_2P_2$ determined with magnetization (110 K) and μ^+SR (85 K) measurements is most likely caused by the effect of an applied external magnetic field. Since the AF order in $CaCo_2P_2$ is an A type [9], the FM order of Co moments is formed in the ab plane. The FM order formation is naturally enhanced with an external magnetic field, which magnetization measurements require. On the contrary, μ^+SR provides the information on an internal magnetic field even in ZF. Therefore, the observed T_N for the A-type order with μ^+SR is lower than that with magnetization measurements.

B. Which moment is responsible?

For x below 0.5, the Eu moments should be responsible for the IC-AF order because T_N decreases monotonically with x and the internal AF field at the lowest temperature, i.e., 2 K, also decreases with x [see Fig. 9(a)]. This implies the dilution effect caused by the Ca substitution for Eu. Since the Eu moment is well localized at the atomic position, such a decrease in T_N in addition to the change from the IC-AF phase to the DO-AF phase could be explained by the percolation theory [35,36]. In fact, the percolation threshold of the magnetic order in the two-dimensional square lattice is predicted as $p_c = 0.593$, which in this case corresponds to $x = 0.407$. Below the percolation limit of Eu^{2+}, i.e., at $0.407 < x$, the Co moments are naturally responsible for the manifestation of the DO-AF phase. This also suggests the absence of any (or negligibly small) interactions between the Eu and Co moments until approximately $x = 0.5$.

The appearance of the DO-FM phase at $0.57 \leqslant x < 0.9$ indicates that the Co^{1+} moments are responsible for the DO-FM phase because the lattice-collapse transition occurs at around $x = 0.55$, leading to the generation of Co^{1+} ions. This also suggests the presence of FM Co-Eu-Co interactions along the c axis that stabilize the DO-FM phase well above T_N. Regardless of its sign, the Co-Eu-Co interaction becomes FM because the spin arrangement of Co-Eu-Co is "-up-up-up-" for the FM Co-Eu coupling, and "-up-down-up-" for the AF Co-Eu coupling. Furthermore, the FM Co-Eu-Co interaction along the c axis is most likely comparable to the AF Co-Co interaction along the c axis. The former interaction is superior at high temperatures, while the latter one is superior at low temperatures. Consequently, a high-temperature DO-FM phase changes to a low-temperature DO-AF phase with decreasing temperature. This situation is very different from that described in the related compound, $EuRbFe_4As_4$ [37], for which the inelastic neutron scattering experiment revealed a very weak coupling between the Eu moment and the Fe moment.

Therefore, the spin Hamiltonian for $Eu_{1-x}Ca_xCo_2P_2$ with $0.57 \leqslant x$ in ZF could be roughly represented by a combination of an intralayer and interlayer coupling between Co moments with $S = 1$, as in the case of other A-type antiferromagnets [38],

$$\mathcal{H} = \boldsymbol{J_{ab}} \sum_{ab} \boldsymbol{S_i S_j} + \boldsymbol{J_c} \sum_{c} \boldsymbol{S_i S_j} \tag{5}$$

and

$$\boldsymbol{J_c} = \boldsymbol{J_{c1}} + \boldsymbol{J_{c2}}, \tag{6}$$

where $\boldsymbol{S}$ denotes the spin operator of Co^{1+} ions with $S = 1$, $\boldsymbol{J_{ab}}$ denotes the intralayer FM exchange, and $\boldsymbol{J_c}$ denotes the interlayer exchange, which should also consist of the following two components: $\boldsymbol{J_{c1}}$ and $\boldsymbol{J_{c2}}$ (Fig. 15). Here, $\boldsymbol{J_{c1}}$ denotes the interlayer AF direct exchange and $\boldsymbol{J_{c2}}$ denotes the interlayer FM indirect exchange through Eu^{2+}. Naturally, when $x = 1$, $\boldsymbol{J_{c1}} \neq 0$ but $\boldsymbol{J_{c2}} = 0$. Considering the distances between the nearest-neighboring Co ions at the ab plane and along the c axis, $\boldsymbol{J_{ab}}$ is most likely predominant in the entire x range. Moreover, $\boldsymbol{J_{c2}}$ is comparable to $\boldsymbol{J_{c1}}$ at around $x = 0.9$. However, it is necessary to perform inelastic neutron experiments on $Eu_{1-x}Ca_xCo_2P_2$ with $0.57 \leqslant x < 0.9$ and $CaCo_2P_2$ to determine each exchange parameter for further discussion.

μ^+SR detected static AF order only at $0.9 \leqslant x \leqslant 1$ and $0 \leqslant x \leqslant 0.4$, implying that the Eu substitution for Ca at $0.9 \leqslant$

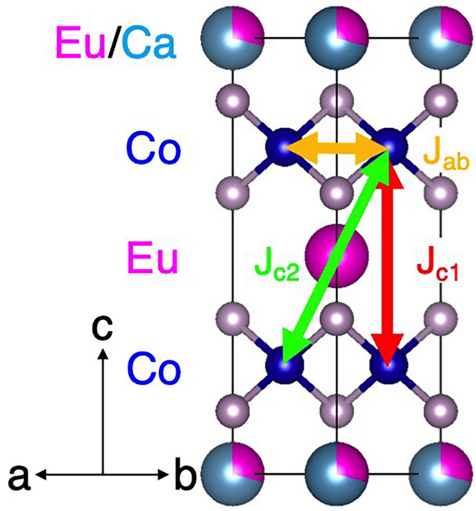

FIG. 15. Possible magnetic interactions, $\boldsymbol{J_{ab}}$, $\boldsymbol{J_{c1}}$, and $\boldsymbol{J_{c2}}$, in $Eu_{0.3}Ca_{0.7}Co_2P_2$. Here, $\boldsymbol{J_{ab}}$ denotes the intralayer FM exchange, $\boldsymbol{J_{c1}}$ denotes the interlayer AF direct exchange, and $\boldsymbol{J_{c2}}$ denotes the interlayer FM indirect exchange through Eu^{2+}, i.e., the Co-Eu-Co exchange. Note that $\boldsymbol{J_{c2}}$ becomes FM regardless of the sign of the Co-Eu exchange.

$x \leqslant 1$ induces not only a mere decrease in the number of Ca ions, but also a local lattice elongation along the c axis. Consequently, the surrounding Co^{+1} ions at the substituted Eu are converted into Co^{+2} ions. A narrow stable range of the A-type AF ordered phase ($0.9 \leqslant x \leqslant 1$) suggests that the one substituted Eu generates multiple Co^{2+} ions.

Since the magnetic order strongly depends on x and the c-axis length, it is highly necessary to investigate the pressure dependence of the magnetic nature of $Eu_{1-x}Ca_xCo_2P_2$ with μ^+SR, similarly to the previous study on $Sr_{1-x}Ca_xCo_2P_2$ [30], particularly at the vicinity of the lattice-collapse transition. Because the maximum pressure for μ^+SR measurements is found around 2.8 GPa [39], it would be difficult to investigate the magnetic nature of $EuCo_2P_2$ under pressure to identify whether the valence state of Eu changes at around 3.1 GPa, as detected with Mössbauer measurements [40] and explained with DFT calculations [41,42].

V. SUMMARY

We studied the microscopic magnetic nature of a solid solution system $Eu_{1-x}Ca_xCo_2P_2$ with a muon spin rotation and relaxation (μ^+SR) technique down to 2 K. Based on weak transverse-field and zero-field μ^+SR measurements, all compounds were found to enter a magnetic phase at low temperatures regardless of x. Particularly at $x = 0.57$, above which the lattice-collapsed tetragonal phase is stabilized, a disordered ferromagnetic (DO-FM) phase appeared at temperatures below 200 K ($= T_C$), which subsequently changed to a DO-AF phase below 60 K ($= T_N$). The magnitude of T_C decreased rapidly with increasing x up to $x = 0.9$, while T_N decreases slowly with x. The DO-FM phase disappeared at $0.9 \leqslant x$, at which point the ordered AF phase appeared. These features suggest the coexistence of two interlayer interactions, namely, a FM $Co^{1+} - Eu^{2+} - Co^{1+}$ interaction through Eu and an AF $Co^{1+} - Co^{1+}$ direct interaction. The competition between these two interactions is most likely to provide a rich magnetic phase diagram on $Eu_{1-x}Ca_xCo_2P_2$.

ACKNOWLEDGMENTS

We would like to thank the staff of TRIUMF (especially the CMMS) for helping us with the μ^+SR experiments (Proposal No. M2177) and Enago [43] for the English language review. All images involving crystal structures were made with VESTA [44]. R.P. was funded by a postdoctoral scholarship awarded by the Dr. Ragnar Holm's Foundation. O.K.F. was supported by the Swedish Research Council (VR) via Grant No. 2022-06217 and the Foundation Blanceflor 2023 fellow scholarship. K.M., K.Yoshinaga, C.M., H.U., and K. Yoshimura were supported by the Japan Society for the Promotion Science (JSPS) KAKENHI Grants No. JP18KK0150 and No. JP22H01761. I.U. was supported by JSPS KAKENHI Grant No. JP22H03875. This work was supported by JSPS KAKENHI Grants No. JP18H01863, No. JP20K21149, and No. JP23H01840.

[1] R. Hoffmann and C. Zheng, J. Phys. Chem. **89**, 4175 (1985).
[2] E. Mörsen, B. Mosel, W. Mürller-Warmuth, M. Reehuis, and W. Jeitschko, J. Phys. Chem. Solids **49**, 785 (1988).
[3] G. Just and P. Paufler, J. Alloys Compd. **232**, 1 (1996).
[4] M. Shatruk, J. Solid State Chem. **272**, 198 (2019).
[5] Y. Lai, J. Y. Chan, and R. E. Baumbach, Sci. Adv. **8**, eabp8264 (2022).
[6] M. S. Torikachvili, S. L. Bud'ko, N. Ni, and P. C. Canfield, Phys. Rev. Lett. **101**, 057006 (2008).
[7] S. Jia, P. Jiramongkolchai, M. R. Suchomel, B. H. Toby, J. G. Checkelsky, N. P. Ong, and R. J. Cava, Nat. Phys. **7**, 207 (2011).
[8] S. Jia, A. J. Williams, P. W. Stephens, and R. J. Cava, Phys. Rev. B **80**, 165107 (2009).
[9] M. Reehuis, W. Jeitschko, G. Kotzyba, B. Zimmer, and X. Hu, J. Alloys Compd. **266**, 54 (1998).
[10] C. Zheng and R. Hoffmann, J. Solid State Chem. **72**, 58 (1988).
[11] D. Johrendt, C. Felser, O. Jepsen, O. K. Andersen, A. Mewis, and J. Rouxel, J. Solid State Chem. **130**, 254 (1997).
[12] A. Teruya, A. Nakamura, T. Takeuchi, H. Harima, K. Uchima, M. Hedo, T. Nakama, and Y. Onuki, J. Phys. Soc. Jpn. **83**, 113702 (2014).
[13] R. E. Baumbach, V. A. Sidorov, X. Lu, N. J. Ghimire, F. Ronning, B. L. Scott, D. J. Williams, E. D. Bauer, and J. D. Thompson, Phys. Rev. B **89**, 094408 (2014).
[14] M. Imai, C. Michioka, H. Ueda, and K. Yoshimura, Phys. Rev. B **95**, 054417 (2017).
[15] J. Sugiyama, H. Nozaki, I. Umegaki, M. Harada, Y. Higuchi, K. Miwa, E. J. Ansaldo, J. H. Brewer, M. Imai, C. Michioka *et al.*, Phys. Rev. B **91**, 144423 (2015).
[16] K. Moriyama, K. Yoshinaga, R. Matsui, C. Michioka, H. Ueda, and K. Yoshimura, J. Phys. Soc. Jpn. **93**, 033702 (2024).

[17] M. Reehuis, W. Jeitschko, M. Möller, and P. Brown, J. Phys. Chem. Solids **53**, 687 (1992).
[18] N. S. Sangeetha, E. Cuervo-Reyes, A. Pandey, and D. C. Johnston, Phys. Rev. B **94**, 014422 (2016).
[19] N. Higa, Q.-P. Ding, M. Yogi, N. S. Sangeetha, M. Hedo, T. Nakama, Y. Onuki, D. C. Johnston, and Y. Furukawa, Phys. Rev. B **96**, 024405 (2017).
[20] N. Higa, Q.-P. Ding, F. Kubota, H. Uehara, M. Yogi, Y. Furukawa, N. Sangeetha, D. Johnston, A. Nakamura, M. Hedo *et al.*, Phys. B: Condens. Matter **536**, 384 (2018).
[21] T. Takeuchi, T. Tahara, T. Kida, Y. Narumi, M. Hagiwara, K. Kindo, W. Iha, Y. Ashitomi, T. Yara, M. Nakashima *et al.*, J. Phys. Soc. Jpn. **90**, 034709 (2021).
[22] R. Marchand and W. Jeitschko, J. Solid State Chem. **24**, 351 (1978).
[23] G. M. Kalvius, D. R. Noakes, and O. Hartmann, *Handbook on the Physics and Chemistry of Rare Earths* (North-Holland, Amsterdam, Holland, 2001), Vol. 32, Chap. 206, pp. 55–451.
[24] A. Yaouanc and P. D. de Réotier, *Muon Spin Rotation, Relaxation, and Resonance, Application to Condensed Matter* (Oxford University Press, New York, 2011).
[25] S. J. Blundell, R. De Renzi, T. Lancaster, and F. L. Pratt, *Muon Spectroscopy: An Introduction* (Oxford University Press, Oxford, 2021).
[26] A. Suter and B. Wojek, Phys. Procedia **30**, 69 (2012).
[27] D. Andreica, Ph.D. thesis, ETH Zurich, 2001.
[28] A. Amato, P. Dalmas de Réotier, D. Andreica, A. Yaouanc, A. Suter, G. Lapertot, I. M. Pop, E. Morenzoni, P. Bonfà, F. Bernardini *et al.*, Phys. Rev. B **89**, 184425 (2014).
[29] P. Bonfà, I. J. Onuorah, and R. D. Renzi, JPS Conf. Proc. **21**, 011052 (2018).
[30] O. K. Forslund, D. Andreica, Y. Sassa, M. Imai, C. Michioka, K. Yoshimura, Z. Guguchia, Z. Shermadini, R. Khasanov, J. Sugiyama *et al.*, Sci. Rep. **12**, 17526 (2022).
[31] N. Higa, Q.-P. Ding, A. Teruya, M. Yogi, M. Hedo, T. Nakama, Y. Onuki, and Y. Furukawa, Phys. Rev. B **98**, 184433 (2018).
[32] J. Sugiyama, W. Higemoto, D. Andreica, O. K. Forslund, E. Nocerino, M. Månsson, Y. Sassa, R. Gupta, R. Khasanov, H. Ohta *et al.*, Phys. Rev. B **103**, 104418 (2021).
[33] O. K. Forslund, D. Andreica, H. Ohta, M. Imai, C. Michioka, K. Yoshimura, M. Månsson, and J. Sugiyama, Phys. Scr. **96**, 125864 (2021).
[34] O. K. Forslund, H. Ohta, K. Kamazawa, S. L. Stubbs, O. Ofer, M. Månsson, C. Michioka, K. Yoshimura, B. Hitti, D. Arseneau *et al.*, Phys. Rev. B **102**, 184412 (2020).
[35] R. J. Birgeneau, R. A. Cowley, G. Shirane, J. A. Tarvin, and H. J. Guggenheim, Phys. Rev. B **21**, 317 (1980).
[36] D. Stauffer and A. Aharony, *Introduction To Percolation Theory: Second Edition* (Taylor & Francis, London, 1992).
[37] K. Iida, Y. Nagai, S. Ishida, M. Ishikado, N. Murai, A. D. Christianson, H. Yoshida, Y. Inamura, H. Nakamura, A. Nakao *et al.*, Phys. Rev. B **100**, 014506 (2019).
[38] M. J. Lewis, B. D. Gaulin, L. Filion, C. Kallin, A. J. Berlinsky, H. A. Dabkowska, Y. Qiu, and J. R. D. Copley, Phys. Rev. B **72**, 014408 (2005).
[39] R. Khasanov, J. Appl. Phys. **132**, 190903 (2022).
[40] M. Chefki, M. M. Abd-Elmeguid, H. Micklitz, C. Huhnt, W. Schlabitz, M. Reehuis, and W. Jeitschko, Phys. Rev. Lett. **80**, 802 (1998).
[41] D. Guenzburger, D. E. Ellis, and J. A. Gómez, Phys. Rev. B **64**, 214418 (2001).
[42] P. H. Andersson, L. Nordstrom, P. Mohn, and O. Eriksson, Phys. Rev. B **65**, 174109 (2002).
[43] See www.enago.jp.
[44] K. Momma and F. Izumi, J. Appl. Crystallogr. **41**, 653 (2008).